Detection of bone marrow metastases in children and young adults with solid cancers with diffusion-weighted MRI

Ali Rashidi[1] · Lucia Baratto[1] · Praveen Jayapal[1] · Ashok Joseph Theruvath[1] · Elton Benjamin Greene[2] · Rong Lu[3] · Sheri L. Spunt[4] · Heike E. Daldrup-Link[1,4,5]

Abstract

Objective To compare the diagnostic accuracy of diffusion-weighted (DW)-MRI with b-values of 50 s/mm^2 and 800 s/mm^2 for the detection of bone marrow metastases in children and young adults with solid malignancies.

Methods In an institutional review board-approved prospective study, we performed 51 whole-body DW-MRI scans in 19 children and young adults (14 males, 5 females; age range: 1–25 years) with metastasized cancers before ($n = 19$ scans) and after ($n = 32$ scans) chemotherapy. Two readers determined the presence of focal bone marrow lesions in 10 anatomical areas. A third reader measured ADC and SNR of focal lesions and normal marrow. Simultaneously acquired ^{18}F-FDG-PET scans served as the standard of reference. Data of $b = 50$ s/mm^2 and 800 s/mm^2 images were compared with the Wilcoxon signed-rank test. Inter-reader agreement was evaluated with weighted kappa statistics.

Results The SNR of bone marrow metastases was significantly higher compared to normal bone marrow on $b = 50$ s/mm^2 (mean ± SD: 978.436 ± 1239.436 vs. 108.881 ± 109.813, $p < 0.001$) and $b = 800$ s/mm^2 DW-MRI (499.638 ± 612.721 vs. 86.280 ± 89.120; $p < 0.001$). On 30 out of 32 post-treatment DW-MRI scans, reconverted marrow demonstrated low signal with low ADC values ($0.385 \times 10^{-3} \pm 0.168 \times 10^{-3}$ mm^2/s). The same number of metastases (556/588; 94.6%; $p > 0.99$) was detected on $b = 50$ s/mm^2 and 800 s/mm^2 images. However, both normal marrow and metastases exhibited low signals on ADC maps, limiting the ability to delineate metastases. The inter-reader agreement was substantial, with a weighted kappa of 0.783 and 0.778, respectively.

Conclusion Bone marrow metastases in children and young adults can be equally well detected on $b = 50$ s/mm^2 and 800 s/mm^2 images, but ADC values can be misleading.

Keywords DW-MRI · b value · Apparent diffusion coefficient · Children · Bone marrow metastases

✉ Heike E. Daldrup-Link
H.E.Daldrup-Link@stanford.edu

1 Department of Radiology, Molecular Imaging Program at Stanford, Stanford University School of Medicine, Stanford, CA, USA

2 Department of Radiology, Pediatric Radiology, Lucile Packard Children's Hospital, Stanford University School of Medicine, Stanford, CA, USA

3 Quantitative Sciences Unit, Stanford University School of Medicine, Stanford, CA, USA

4 Department of Pediatrics, Hematology/Oncology, Stanford University School of Medicine, Stanford, CA, USA

5 Department of Radiology, Lucile Packard Children's Hospital, Stanford University School of Medicine, 725 Welch Rd, Stanford, CA 94305-5654, USA

Introduction

Diffusion-weighted magnetic resonance imaging (DW-MRI) or diffusion-weighted imaging (DWI) has been used for the detection and treatment monitoring of bone marrow lesions in adults [1–3] and children [4–6]. DW-MRI is based on the principle of random motion of free water molecules in the biological tissues, and it depends on various factors such as intracellular vs extracellular water, type of tissues, and cell density [7]. However, the relationship between cell density and water diffusion of normal and neoplastic bone marrow in children is a relatively understudied area, despite an emerging appreciation of the close link between these two biological variables [2, 8, 9]. Previous investigators reported that proton diffusion is inversely related to tumor cell size and density, and directly related to the size of the extracellular

space [9]. The vast majority of malignant tumors in children are high-grade tumors, which show markedly restricted diffusion on DW-MRI scans [10]. However, in children, normal hypercellular marrow can also demonstrate restricted diffusion with low apparent diffusion coefficient (ADC) values [11]. Chemotherapy can lead to a transiently increased cell density of the normal reconverted bone marrow, thereby causing diffusion restriction and low ADC values. Also, red marrow reconversion changes can mask the detection of focal lesions on T1- and T2-weighted MRI scans [12]. Co-treatment with drugs that stimulate the reconversion of normal hematopoietic marrow (e.g., granulocyte colony-stimulating factor, GCSF) can further amplify this effect [13]. We previously reported that DW-MRI can detect lesions in reconverted marrow in children that have been missed on ^{18}F-FDG-PET [14]. However, to our knowledge, nobody has yet determined the optimal pulse sequence parameters for the detection of bone marrow metastases with DW-MRI in children and young adults.

In children, Grasparil et al. compared the sensitivity and specificity of DW-MR images with a b-value of 50 s/mm^2 and 600 s/mm^2 for the detection of metastases in the liver [15]. Surprisingly, the team found a higher sensitivity of $b = 50$ s/mm^2 images compared to $b = 600$ s/mm^2 images for the detection of liver lesions. It is possible that the combined T2 effects and DWI signal of malignant lesions on $b = 50$ s/mm^2 images provided a better contrast-to-noise ratio. Another explanation might be a lower confounding effect of intrinsic iron in patients who are receiving blood transfusions, such as patients with neuroblastoma or leukemia, on $b = 50$ s/mm^2 images. Both of these effects could also apply to other organs of the reticuloendothelial system, such as the bone marrow. However, no related information regarding the detection of bone marrow metastases on DW-MRI exists to date.

The purpose of this study was to close this gap by comparing the diagnostic accuracy of diffusion-weighted MRI with the b-values of 50 s/mm^2 and 800 s/mm^2 for the detection of bone marrow metastases in children and young adults with solid malignant tumors.

Materials and methods

Patient population

This prospective non-randomized, Health Insurance Portability and Accountability Act (HIPAA)–compliant clinical trial was approved by the institutional review board at our institution (IRB20221 and IRB44706). We enrolled 19 pediatric patients and young adults with biopsy-proven cancers, including 14 males and 5 females with an age of 5–25 years, mean age ($\pm$ standard deviation [SD]) 15.7 ± 5.4 years,

from June 2018 until December 2021 (Fig. 1). Fifteen patients were below the age of 18 (15/19, 79%) and four patients were older than 18 years (4/19, 21%) at enrollment. Informed consent was obtained from all individual participants > 18 years. From all individual participants < 18 years, assent was obtained, and consent was obtained from their parents or legal guardians. Inclusion criteria comprised biopsy-proven diagnosis of a solid extracranial malignant tumor in patients with an age of 1–25 years, and the diagnosis of bone marrow metastases, based on a bone marrow biopsy ($n = 5$) or imaging (including x-rays, CT, MRI, FDG-PET, bone scan, $n = 14$) within 6 months after the end of chemotherapy. Exclusion criteria comprised MRI contraindications, such as claustrophobia, the presence of ferromagnetic prostheses, pacemakers, or other implants incompatible with MRI. Patients' characteristics are detailed in Table 1.

Image acquisition

All patients underwent a whole-body DW-MRI scan on a GE Signa 3 T PET/MR scanner (GE Healthcare, Milwaukee, WI), using the multi-channel surface coils for the head, chest, abdomen, and extremities. Our 19 patients received 51 scans, which included 19 scans at baseline, 19 scans at the end of their chemotherapy, and 13 scans at 2–6 months after the end of the chemotherapy (mean $\pm$ SD: 3.3 ± 1.5 months).

Whole-body axial DW-MR images, covering the vertex to the toes, were obtained with a repetition time (TR) = 7824 ms, echo time (TE) = 56 ms, slice thickness (SL) = 6 mm, field of view (FOV) = 48 cm, b-value = 50/800 s/mm^2, a matrix of 80×128 pixels, and an acquisition time (TA) of 1:47 min. In addition, we acquired pre- and post-contrast whole-body T1-weighted Liver Acquisition with Volume Acquisition sequences (LAVA, alpha = 15 degrees, TR = 4364 ms, TE = 1674 ms, SL = 0.88 mm, FOV = 48 cm, Matrix = 320×256 pixels, and TA = 3:21 min). Intravenous injection of gadobutrol (Gadavist, Gd; 0.1 mL/kg body weight (0.1 mmol/kg)) was utilized for post-contrast imaging. All images were acquired in the axial plane. Post-contrast images were also reconstructed in the coronal plane. We reconstructed ADC maps from DW-MR images (b-values = 50 s/mm^2 and 800 s/mm^2) using the scanner software (3 T Signa PET/MR, software version MP26, GE Healthcare, Milwaukee, WI). For the reconstruction of ADC maps, b = 0 s/mm^2 was not included.

Simultaneously with the DW-MRI scan, patients received a whole-body ^{18}F-labeled fluorodeoxyglucose enhanced positron emission tomography (^{18}F-FDG-PET) scan, covering from the vertex to the toes (FOV = 48 cm, SL = 2.8 mm, and TA = 3:30 min), which was acquired at 60 min after intravenous injection of ^{18}F-FDG at a dose of 3 MBq/kg body weight.
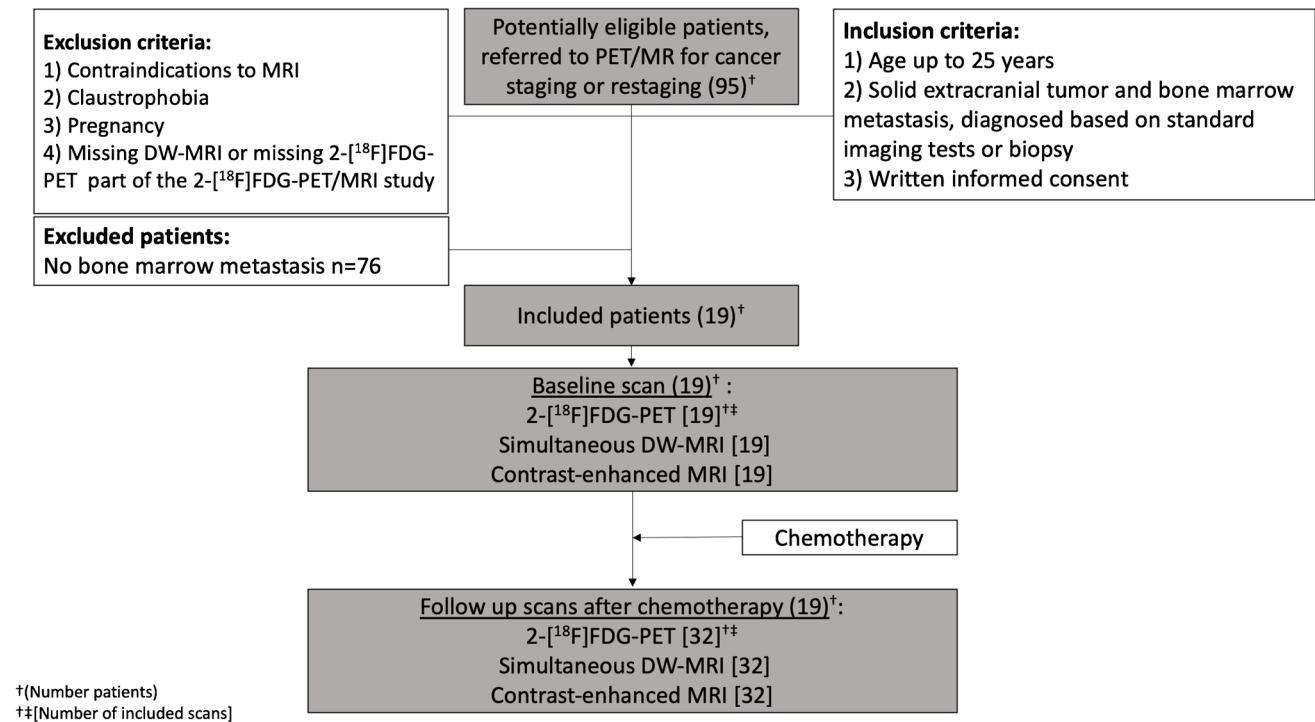
Fig. 1 The flow diagram of the participants. Among 95 potentially eligible patients who were referred to PET/MR for cancer staging or restaging, and based on the inclusion and exclusion criteria, 19 children and young adult patients were included in the study and underwent simultaneous ^{18}F-FDG-PET, DW-MRI, and contrast-enhanced MRI scans at baseline and after receiving treatment. Our 19 patients received 51 scans: 19 scans at baseline and 32 scans after chemotherapy, which included, 19 scans at the end of their chemotherapy, and 13 scans at 2–6 months after the end of the chemotherapy

Image analyses

Two reviewers (HEDL and EBG with > 20 years and 6 years of experience, respectively, in interpreting whole-body MRI), who were blinded to clinical information, independently recorded the presence or absence of focal bone marrow lesions in 10 anatomical regions in DW-MRI. These anatomical regions included the head (calvarium and face), spine (cervical, thoracic, and lumbar), ribs/clavicles, bilateral humerus, radius/ulna, hands, pelvis, femurs, tibia/fibula, and feet. A focal bone marrow metastasis was defined as a focal lesion in the bone marrow with a hyperintense signal compared to adjacent skeletal muscle on DWI and a low signal on the corresponding ADC map. The bone marrow lesions were measured using the longest axis of each lesion and based on the diameter of the lesions were divided into ≥ 10 mm or < 10 mm.

The confidence of the reviewers regarding their diagnosis was graded according to a Likert scale as follows: 1 = definitely not present, 2 = probably not present, 3 = undecided, 4 = probably present, and 5 = definitely present. The simultaneously acquired ^{18}F-FDG-PET data were used as a standard of reference for MRI findings.

On ^{18}F-FDG-PET scans, bone marrow metastasis was defined based on increased metabolic activity compared to adjacent normal bone marrow. We determined the SUV value of reference lesions in the bone marrow; all lesions had an SUV value above that of the liver as an internal reference standard. However, we did not use a cutoff value. A separate panel of two reviewers (LB, a nuclear medicine physician, and PJ, a radiologist, with 6 and 3 years of experience, respectively, in interpreting cross-sectional scans) determined the standard of reference in consensus. The reference standard was determined before reading the DW-MRI images, and readers of DW-MRI images were blinded to the standard of reference findings.

Using the ADC map, tissue diffusion in one representative bone marrow lesion in the central skeleton and the normal bone marrow in the central skeleton (either the pelvis or a lower lumbar vertebral body) was measured. The L3-L5 was interpreted as "lower lumbar." For this purpose, one additional reviewer, a radiologist (AJT, with five years of experience in interpreting whole-body MRI) measured ADC_{mean} and ADC_{min} of the largest bone marrow metastasis and ADC_{mean} of normal bone marrow on ADC maps through operator-defined regions of interest (ROIs) using OsiriX software (version 10.0,

Table 1 Participant demographic

Characteristic	Value (%)
Age (year)	
Mean ± standard deviation	15.7 ± 5.4
Range	5–25
Sex [$n = 19$]	
Female	5 (26)
Male	14 (74)
Tumor type (primary location of tumor) [$n = 19$]	
Sarcoma	8 (43)
Ewing sarcoma (scapula, rib, humerus)	3
Osteosarcoma (femur, humerus, pelvis)	3
Rhabdomyosarcoma (neck)	1
Desmoplastic small round cell tumor (abdomen)	1
Lymphoma	7 (37)
Hodgkin lymphoma	6
Non-Hodgkin lymphoma	1
Carcinoma	2 (10)
Choriocarcinoma (testes)	1
Large cell neuroendocrine carcinoma (lung)	1
Wilms tumor	1 (5)
Neuroblastoma	1 (5)
Scans, treatment status [$n = 51$]	
Baseline	19 (37)
Post-treatment	32 (63)

64 bit; Pixmeo, Geneva, Switzerland). The ROI for measurement of a bone marrow lesion was placed such that it covered the entire lesion with an area of 10 mm^2. The normal bone marrow was measured with an ROI with an area of 10 mm^2 at the same slice of the bone marrow lesion. In addition, the signal-to-noise ratio (SNR = MRI signal intensity/background noise standard deviation) of the same lesion and normal bone marrow was measured through operator-defined ROIs on DW images using OsiriX software (version 10.0, 64 bit; Pixmeo, Geneva, Switzerland). Similar to ADC measurements, the ROI for measurement of a bone marrow lesion was placed such that it covered the entire lesion with an area of 10 mm^2. The normal bone marrow was measured with an ROI with an area of 10 mm^2 at the same slice of the bone marrow lesion. The background noise standard deviation was measured by placing the same ROI in the background air exterior of the patient and at the level of the bone marrow lesion. The contrast of bone marrow metastases (met) regarding the normal bone marrow (BM) was calculated as follows:

$$ADC\ lesion\ to\ marrow\ contrast(\%) = \frac{(ADCmin met - ADCmean BM) \times 100}{ADCmean BM}$$

$$SNR lesion to marrow contrast(\%) = \frac{(SNR met - SNR BM) \times 100}{SNR BM}$$

In our study, all osseous metastases were primary bone marrow metastases or bone marrow metastases with cortical involvement. We did not encounter any isolated osseous cortical metastasis.

Power analysis

To control the entire study's overall type one error rate at 5%, hypothesis testing of continuous outcome was considered significant if FDR-adjusted p-value < 0.049, while testing of binary outcome was considered significant if FDR-adjusted p-value < 0.001. The FDR-adjusted p-value is referring to the adjusted p-values for multiple comparisons using Benjamini and Hochberg's method [16]. Because we set a more stringent threshold on type I error for tests of binary outcomes, hypothesis testing of binary outcomes should have lower power compared to tests of continuous outcomes. We performed the power analysis to explore the lower bound of the statistical power of the study. This power analysis was performed during the study design phase, without knowing how many follow-up time points we could get for each individual patient. Two-time points were considered as the minimum sample size required for each patient, to ensure that each patient can have at least one baseline measure and one post-treatment measure.

Based on 1000 simulations using the Generalized Linear Mixed Models (GLMM) with a binary outcome and logit link, if 10 regions from each scan will be used for comparing diagnostic accuracy, in order to detect > 6SD b-value effect, out of total 7SD fixed effects, with 83.7% power (95% CI: 81.26–85.94%) and 0.1% type I error, at least 18 patients need to be scanned using both methods at ≥ 2-time points, where SD = 1 is the standard deviation of the random-intercept effect within each patient. Under the assumptions that the true fixed intercept effect is 1SD and the true method/b-value effect is 4SD (instead of 6SD), 18 patients scanned using both methods at ≥ 2-time points can provide 75.40% power (95% CI: 72.61–78.04%) when type I error is set at 0.1%. This power analysis was performed using the R package *simr* [17].

Statistical analyses

Continuous data were summarized as means and SD. To calculate the sensitivity, specificity, and diagnostic accuracy, we performed a "region-based" analysis, which allowed us to designate the above-mentioned 10 regions per patient as true positive, true negative, false positive, or false negative according to the reference standard. If at least one lesion was missed in a given region with more than one lesion, then this region was counted as a "false negative." Sensitivities,

specificities, and diagnostic accuracies of DW-MRI with b-values of the 50 s/mm^2 and 800 s/mm^2 were compared using a Generalized Estimation Equation (GEE). For comparison of these values, 19 scans at baseline and 19 scans at the end of the chemotherapy were compared with the reference standard at each time point. In addition, we separately analyzed the results of 19 baseline scans and 13 post-treatment scans to determine if the status pre/post-chemotherapy would affect our results.

The Wilcoxon signed-rank test was utilized to compare the ADC values of the normal bone marrow and metastases before and after chemotherapy and the ADC lesion-to-marrow contrast. Also, the SNR values of the normal bone marrow and metastases before and after chemotherapy and the SNR lesion-to-marrow contrast were compared by Wilcoxon signed-rank test. The inter-reader agreement in the assessment of the Likert scale for actual lesion detection on a lesion-by-lesion basis, using the above-mentioned standard of reference, was evaluated by weighted kappa statistics, according to Cohen and Landis [18, 19]. The confidence of reviewers in the delineation of bone marrow lesions and normal bone marrow was compared by the chi-square test. For this test, the Likert scales of 1 = definitely not present and 5 = definitely present were considered as "definite," and the Likert scales of 2 = probably not present, 3 = undecided, and 4 = probably present, were considered as "probable." Also, the confidence of reviewers in the delineation of bone marrow lesions with a size of ≥ 10 mm or < 10 mm was compared by the Chi-square test. All statistical analyses were performed using Statistical Package for Social Sciences software (IBM SPSS Statistics for Mac, Version 28.0., Armonk, NY: IBM Corp.).

Results

At baseline, 13/19 patients (68.4%) demonstrated a lower signal compared to muscle as an internal standard on T1-weighted gradient echo images as well as a low signal on DW-MR images ($b = 50$ s/mm^2: 108.881 ± 109.813; $b = 800$ s/mm^2: 86.280 ± 89.120, Fig. 2). ^{18}F-FDG-PET images demonstrated low metabolic activity of the normal bone marrow. On interim follow-up scans (2–8 weeks after chemotherapy), 17/19 patients demonstrated low bone marrow signal on 30/32 post-treatment DW-MR images ($b = 50$ s/mm^2: 92.552 ± 79.556; $b = 800$ s/mm^2: 65.736 ± 54.854), while 2 patients demonstrated restricted diffusion of the entire bone marrow on $b = 800$ s/mm^2 images, but not $b = 50$ s/mm^2 images (Fig. 2). At 6 months after chemotherapy, all patients demonstrated low bone marrow signals on DW-MR images.

MRI signal of focal lesions and normal marrow on DW-MRI

According to the standard of reference, our patients had 588 bone marrow metastases. DW-MRI with b values of 50 s/mm^2 and 800 s/mm^2 both detected 556 of the 588 lesions (94.6%, Table 2). Sensitivities (96.6%), specificities (100%), and diagnostic accuracies (99.0%) were not different for DW-MR images with a b-value of 50 s/mm^2 and 800 s/mm^2, either before (sensitivity: 96.8%, specificity: 100%, and diagnostic accuracy: 98.9%, respectively) or after chemotherapy (sensitivity: 96.3%, specificity: 100%, and diagnostic accuracy: 99.1%, respectively; all $p > 0.99$, Table 3).

The reported Likert scales for $b = 50$ s/mm^2 and $b = 800$ s/mm^2 images were not significantly different (2.090 ± 1.706 vs. 2.095 ± 1.712, respectively, $p > 0.99$). Bone marrow lesions with a size of less than 1 cm were detected with similar confidence on $b = 50$ s/mm^2 images (3.100 ± 1.919) and $b = 800$ s/mm^2 images (3.080 ± 1.914, $p > 0.99$). Similarly, bone marrow lesions with a size of 1 cm and more were detected with similar confidence on $b = 50$ s/mm^2 images and $b = 800$ s/mm^2 images (both 4.180 ± 1.547). However, three bone marrow lesions, one in the pelvis (Fig. 3) and two in the femur, and all on post-treatment scans were better detected on $b = 50$ s/mm^2, and three bone marrow lesions in the spine, one lesion on the baseline and two lesions on post-treatment scans, were better detected on $b = 800$ s/mm^2 (Fig. 4). The better detection of lesions on $b = 50$ s/mm^2 was due to the increased proton content and/or necrosis of lesions after chemotherapy (Fig. 3), while the better detection of spinal lesions on $b = 800$ s/mm^2 was in part due to suppression of T2 shine-through effects of the cerebrospinal fluid (Fig. 4). The inter-reader agreement in the assessment of the Likert scale for actual lesion detection on a lesion-by-lesion basis for both $b = 50$ s/mm^2 and $b = 800$ s/mm^2 was substantial, with a weighted kappa of 0.783 and 0.778, respectively.

ADC values of the normal bone marrow and metastases before and after chemotherapy

Before chemotherapy, the ADC$_{mean}$ of the normal bone marrow ranged from 0.208 to 0.836 × 10^{-3} mm^2/s with a mean (± SD) value of 0.383 × 10^{-3} ± 0.147 × 10^{-3} mm^2/s. After chemotherapy, the ADC$_{mean}$ of the normal bone marrow ranged from 0.087 to 0.789 × 10^{-3} mm^2/s with a mean value of 0.385 × 10^{-3} ± 0.168 × 10^{-3} mm^2/s. The ADC values of the normal bone marrow before and after chemotherapy were not significantly different ($p = 0.756$; Figs. 2 and 5).

The ADC values of bone marrow metastases were significantly higher compared to the normal bone marrow, both at baseline and on follow-up studies: Before
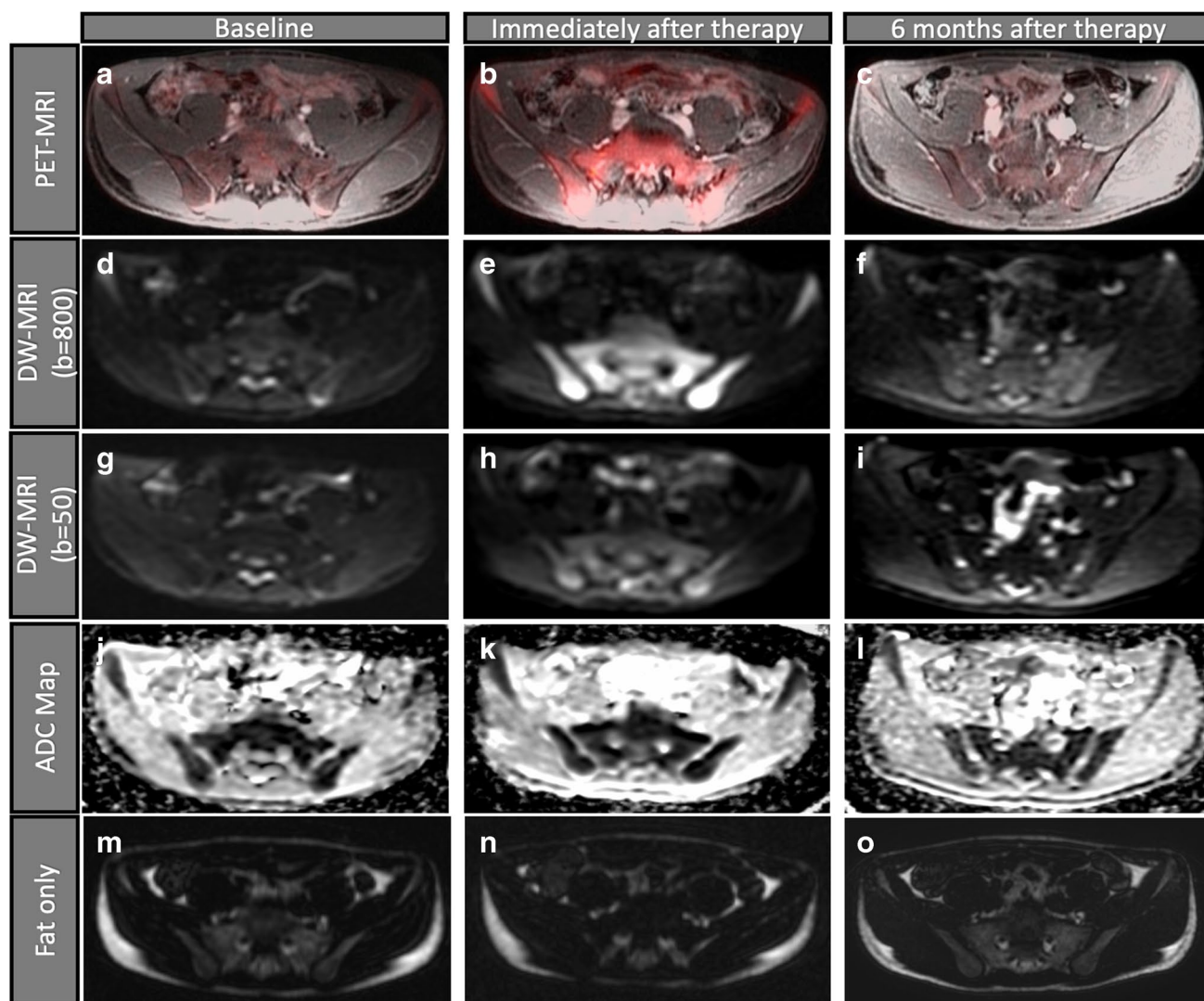
Fig. 2 Therapy-induced bone marrow reconversion in a 16-year-old boy with large cell neuroendocrine carcinoma of the lung. ^{18}F-FDG-PET-MRI demonstrates a low metabolic activity of the normal bone marrow of the iliac bones and sacrum at baseline (**a**). Immediately (24 h) after therapy, hypermetabolic marrow is appreciated (**b**), while after 6 months of therapy, the bone marrow metabolic activity returns to normal (**c**). The simultaneous DW-MRI demonstrates a similar pattern with restricted diffusion immediately after treatment and relatively less diffusion restriction at baseline and after 6 months of therapy on both $b = 800$ s/mm^2 (**d, e, f**) and $b = 50$ s/mm^2 (**g, h, i**). DW-MRI with b = 800 s/mm^2 shows higher signal intensity of reconverted marrow compared with $b = 50$ s/mm^2 images immediately after therapy (**e** and **h**, respectively), suggesting that the observed effects are due to increased bone marrow cellularity rather than edema. However, the ADC map demonstrates a similar pattern of bone marrow on baseline (**j**), immediately (**k**), and 6 months after therapy (**l**) scans. The corresponding fat-only images from the Dixon sequence demonstrate normal intermediate signal intensity of the bone marrow at baseline (**m**), decreased signal intensity immediately after therapy, apparently indicating decreased fat content and increased cellularity of the reconverted marrow (**n**), and increasing signal at 6 months after therapy, apparently indicating increasing fact content and decreasing cellularity of normal marrow (**o**)

chemotherapy, the mean ADC$_{mean}$ of bone marrow metastases was 0.967×10^{-3} mm^2/s $\pm 0.438 \times 10^{-3}$ mm^2/s (ranging from 0.488 to 1.999×10^{-3} mm^2/s) and the mean ADC$_{mean}$ of the normal bone marrow was 0.383×10^{-3} mm^2/s; ($p < 0.001$; Fig. 2). After chemotherapy, the mean ADC$_{mean}$ of bone marrow metastases was $1.379 \times 10^{-3} \pm 0.638 \times 10^{-3}$ mm^2/s (ranging from 0.552 to 2.272×10^{-3} mm^2/s), and the mean ADC$_{mean}$ of the normal bone marrow was $0.385 \times 10^{-3} \pm 0.168 \times 10^{-3}$ mm^2/s ($p < 0.001$; Fig. 5).

The ADC lesion-to-marrow contrast after chemotherapy was significantly higher compared to the scans before treatment (mean $\pm$ SD: 181.414 ± 151.907 vs. 50.671 ± 94.954, respectively, $p = 0.015$, Fig. 6).

Table 2 The number of bone marrow metastases detected on DW-MRI (b=50 s/mm^2) and DW-MRI (b=800 s/mm^2) scans according to the standard of reference

Bone marrow lesions	Image modality	Total[*] [% of detected lesions]	Baseline [% of detected lesions]	Post-treatment [% of detected lesions]
< 10 mm	DW-MRI (b=50 s/mm^2)	221 [89.1]	97 [85.0]	124 [92.5]
	DW-MRI (b=800 s/mm^2)	221 [89.1]	97 [85.0]	124 [92.5]
	^{18}F-FDG-PET[b]	248	114	134
≥ 10 mm	DW-MRI (b=50 s/mm^2)	335 [98.5]	151 [96.8]	184 [100]
	DW-MRI (b=800 s/mm^2)	335 [98.5]	151 [96.8]	184 [100]
	^{18}F-FDG-PET	340	156	184
All lesions	DW-MRI (b=50 s/mm^2)	556 [94.6]	248 [91.9]	308 [96.9]
	DW-MRI (b=800 s/mm^2)	556 [94.6][a]	248 [91.9]	308 [96.9]
	^{18}F-FDG-PET	588	270	318

[*] Detected lesions were identical for both readers

[a] No statistically significant difference when compared with DW-MRI (b=50 s/mm^2) (p>.99)

[b] The ^{18}F-FDG-PET data were used as a standard of reference for MRI findings

[#]Two reviewers independently recorded the presence or absence of focal bone marrow lesions. The discrepancies were resolved by consensus reading of two readers. The reported number of lesions is after resolving the discrepancies by consensus reading of two readers

Abbreviations: *DW-MRI*, diffusion weighted-magnetic resonance imaging

SNR values of the normal bone marrow and metastases before and after chemotherapy

Before chemotherapy, focal bone marrow metastases demonstrated hyperintense signal compared to normal bone marrow on DWI (SNR mean ± SD: b = 50: 978.436 ± 1239.436 vs. 108.881 ± 109.813; b = 800: 499.638 ± 612.721 vs. 86.280 ± 89.120, respectively, p < 0.001, Fig. 4). After chemotherapy, focal bone marrow metastases also demonstrated an overall hyperintense signal compared to normal bone marrow on DWI (SNR mean ± SD: b = 50: 1328.606 ± 1082.894 vs. 136.278 ± 186.238; b = 800: 349.831 ± 285.688 vs. 98.217 ± 131.64, respectively, p < 0.001). In some cases, the DWI signal of the lesion decreased, apparently due to treatment-induced tumor cell death. In other cases, the tumor signal increased, possibly due to treatment-induced edema or necrosis (Fig. 3).

At b = 50 s/mm^2, before chemotherapy, the SNR of the bone marrow metastases (SNR mean ± SD = 978.436 ± 1239.436) was significantly higher compared to the SNR of normal bone marrow (108.881 ± 109.813, p < 0.001). After chemotherapy, also, the SNR of the bone marrow metastases (1,328.606 ± 1082.894) was significantly higher compared to the SNR of normal bone marrow (136.278 ± 186.238, p < 0.001). The SNR values of the normal bone marrow and the bone marrow metastases before and after chemotherapy were not significantly different (p = 0.344 and p = 0.554, respectively; Fig. 5).

At b = 800 s/mm^2, before chemotherapy, the SNR of the bone marrow metastases (499.638 ± 612.721) was significantly higher compared to the SNR of normal bone marrow (86.280 ± 89.120; p < 0.001; Fig. 5). After chemotherapy, the SNR of the bone marrow metastases (349.831 ± 285.688) was significantly higher compared to the SNR of normal bone marrow (98.217 ± 131.64; p < 0.001; Fig. 5). The SNR values of the normal bone marrow before and after chemotherapy was not significantly different (p = 0.210). However, the SNR values of the bone marrow metastases were significantly higher before chemotherapy when compared with the SNR values of the bone marrow metastases after chemotherapy (p = 0.028; Fig. 5).

The lesion-to-marrow contrast before and after chemotherapy was not significantly different in b = 50 s/mm^2 (1039.622 ± 735.593 vs. 1641.807 ± 1305.191, respectively, p = 0.076) and b = 800 s/mm^2 (621.919 ± 388.288 vs. 462.786 ± 341.475, respectively, p = 0.653; Fig. 6). However, the lesion-to-marrow contrast was significantly higher on b = 50 s/mm^2 compared to b = 800 s/mm^2 DW-MRI (1039.622 ± 735.593 vs. 621.919 ± 388.288, respectively, p = 0.009; Fig. 7). Similarly, after chemotherapy, the lesion-to-marrow contrast was significantly higher on b = 50 s/mm^2 compared to b = 800 s/mm^2 (1641.807 ± 1305.191 vs. 462.786 ± 341.475, respectively, p < 0.001; Fig. 7). These results reflect that b = 50 s/mm^2 provides better lesion-to-marrow contrast both before and after chemotherapy.

Table 3 Diagnosis of bone marrow metastases on DW-MRI ($b=50$ s/mm2) and DW-MRI ($b=800$ s/mm2) scans according to the standard of reference, based on reviewer assignments of 510 anatomical regions[*] and per region analysis

Treatment status	Image modality	TP	FN	FP	TN	Sensitivity (CI) (%)	Specificity (%)	PPV (%)	NPV (CI) (%)	Accuracy (CI) (%)
Baseline	DW-MRI ($b=50$ s/mm²)	61	2	0	127	96.8 (89.0–99.6)	100	100	98.4 (94.2–99.6)	98.9 (96.2–99.8)
	DW-MRI ($b=800$ s/mm²)	61	2	0	127	96.8 (89.0–99.6)[a]	100	100	98.4 (94.2–99.6)	98.9 (96.2–99.8)
	¹⁸F-FDG-PET[b]	63	0	0	127	100	100	100	1.000	100
Post-treatment	DW-MRI ($b=50$ s/mm²)	79	3	0	238	96.3 (89.6–99.2)	100	100	98.8 (96.3–99.5)	99.1 (97.2–99.8)
	DW-MRI ($b=800$ s/mm²)	79	3	0	238	96.3 (89.6–99.2)[a]	100	100	98.8 (96.3–99.5)	99.1 (97.2–99.8)
	¹⁸F-FDG-PET	82	0	0	238	100	100	100	100	100
All lesions	DW-MRI ($b=50$ s/mm²)	140	5	0	365	96.6 (92.1–98.8)	100	100	98.6 (96.8–99.4)	99.0 (97.7–99.7)
	DW-MRI ($b=800$ s/mm²)	140	5	0	365	96.6 (92.1–98.8)[a]	100	100	98.6 (96.8–99.4)	99.0 (97.7–99.7)
	¹⁸F-FDG-PET	145	0	0	365	100	100	100	100	100

[*] This is a region-based analysis. Ten anatomical regions were evaluated per scan

[a] No statistically significant difference when compared with DW-MRI ($b=50$ s/mm²) ($p>.99$)

[b] The ¹⁸F-FDG-PET data were used as a standard of reference for MRI findings

[#] Two reviewers independently recorded the presence or absence of focal bone marrow lesions in 10 anatomical regions. The discrepancies were resolved by consensus reading of two readers. The reported number of lesions is after resolving the discrepancies by consensus reading of two readers

Abbreviations: *CI*, confidence interval; *DW-MRI*, diffusion-weighted magnetic resonance imaging; *TP*, true positive; *FN*, false negative; *FP*, false positive; *TN*, true negative; *PPV*, positive predictive value; *NPV*, negative predictive value
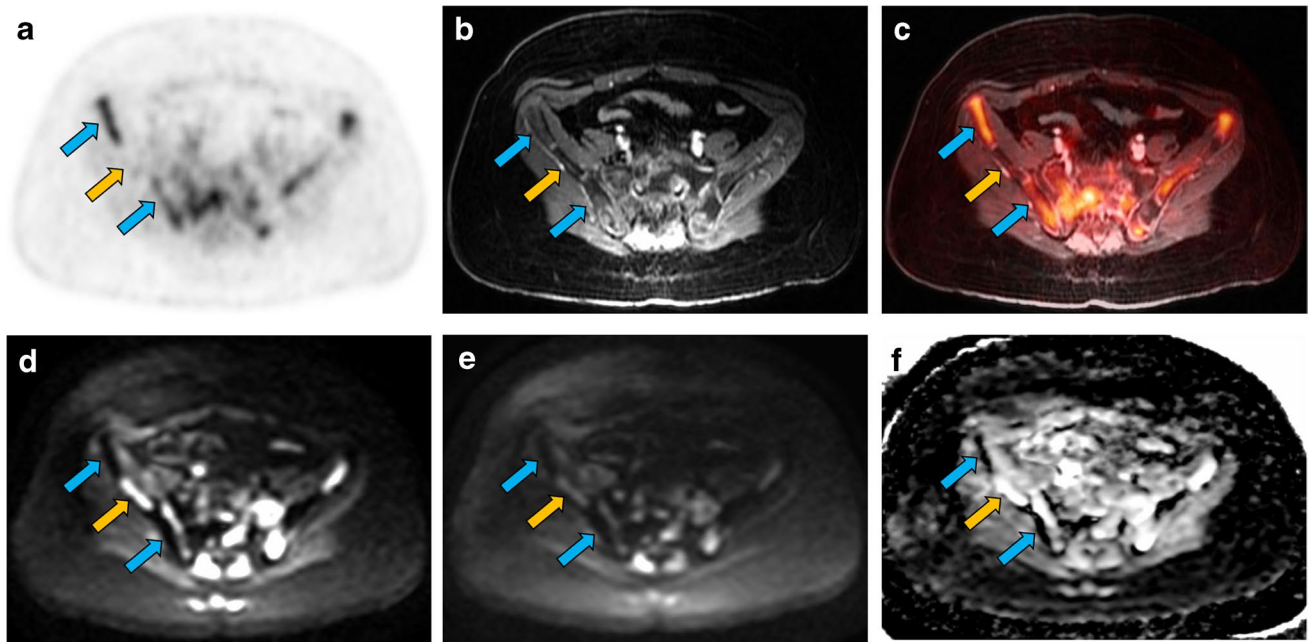
Fig. 3 Inverse signal intensity of reconverted bone marrow on ^{18}F-FDG-PET and DW-MRI scans on the post-treatment scan of a 14-year-old boy with Ewing sarcoma. After chemotherapy, normal bone marrow demonstrates hypermetabolic activity with high FDG uptake on ^{18}F-FDG-PET (**a,** blue arrows) and combined ^{18}F-FDG-PET-MRI (**c,** blue arrows), while a bone marrow metastasis in the right iliac wing demonstrates low FDG uptake (**a** and **c,** yellow arrows). On post-contrast T1-weighted MRI, bone marrow metastasis and normal bone marrow demonstrate no significant contrast enhancement (**b,** blue and yellow arrows). Note the irregular enhancement of the posterior iliac spine bilaterally after bone marrow aspirations. However, on DW-MRI, reconverted bone marrow shows hypointense signal on both $b = 50$ s/mm^2 (**d,** blue arrows), $b = 800$ s/mm^2 (**e,** blue arrows), and the corresponding ADC map (**f,** blue arrows), while the bone marrow metastasis demonstrates hyperintense signal (**d, e,** and **f,** yellow arrows). Also, the bone marrow lesion could be better detected on DW-MRI with a $b = 50$ s/mm^2 (**d,** yellow arrow), compared to $b = 800$ s/mm^2 (**e,** yellow arrow) due to the increased water content or necrosis of the lesion after chemotherapy

Discussion

Our data show that the diagnostic accuracy of diffusion-weighted MR images with b-values of 50 s/mm^2 and 800 s/mm^2 is equal for the detection of bone marrow metastases in children and young adults.

The detection of bone marrow metastases upstages the patient and leads to changes in patient management [20, 21]. Therefore, it is very important to provide accurate bone marrow staging for patients with cancer. In the past, bone marrow involvement in most solid pediatric cancers was diagnosed by bone marrow biopsy [22]. However, since ^{18}F-FDG-PET can sample whole bone marrow non-invasively and with high sensitivity, ^{18}F-FDG-PET scans have replaced bone marrow biopsies for bone marrow staging in children with Hodgkin lymphoma [23]. Several studies reported sensitivities and specificities of ^{18}F-FDG-PET close to 100% [24, 25]. However, the normal hematopoietic marrow in children is characterized by a high cellular density and intrinsic iron content [26]. The iron content in the marrow can increase, especially if blood transfusions are administered during treatment. After chemotherapy, the cell density can temporarily increase (reconverted marrow),

then decrease. Our results show that DW-MRI can delineate focal bone marrow lesions even in reconverted hematopoietic marrow and marrow with high iron content.

We found a mean ADC of $0.383 \times 10-3$ mm^2/s before chemotherapy and $0.385 \times 10-3$ mm^2/s after chemotherapy for the normal bone marrow. The cellularity of the normal bone marrow of children decreases over time by increasing age, resulting in the replacement of the hypercellular red marrow with fatty yellow marrow (fatty conversion) [12]. These age-related changes affect the ADC values of the normal bone marrow of pediatric patients. Nonomura et al. reported the mean ADC value of $1.29 \pm 0.591 \times 10-3$ mm^2/s for normal bone marrow in children with a mean age of 1.6 years [11], and Ibrahim et al. reported that the normal marrow ADC value ranged from 0.902 to $1.34 \times 10-3$ mm^2/s with a mean value of $1.2 \times 10-3$ mm^2/s in children with the mean age of 6.5 years [27], while in children with the mean age of 10.2 years, Tschischka et al. reported the mean ADC value of $0.60 \pm 0.09 \times 10-3$ mm^2/s for normal bone marrow [28]. Our patient cohort included more adolescent patients with a mean age of 15.7 ± 5.4; fifteen patients below the age of 18, and four patients older than 18 years at enrollment. Thus, considering differences in MRI parameters (including
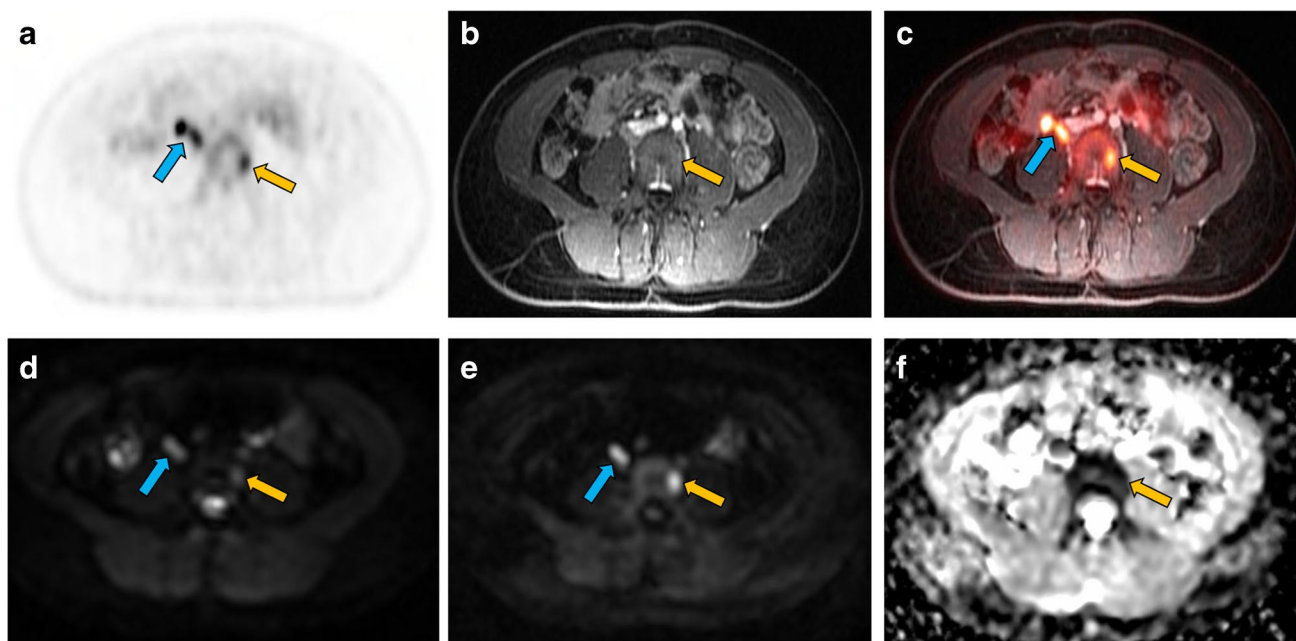
Fig. 4 Better detection of a vertebral bone marrow metastasis in a 17-year-old girl with Hodgkin lymphoma on baseline DW-MRI with a $b=800$ s/mm^2 compared to $b=50$ s/mm^2. ^{18}F-FDG-PET scan demonstrates high FDG uptake of a focal bone marrow metastasis in a lumbar vertebral body (**a,** yellow arrow) and mild FDG uptake of the normal bone marrow. Note also ^{18}F-FDG uptake of retroperitoneal lymph nodes (**a,** blue arrow). While the bone marrow lesion does not enhance on the post-contrast T1-weighted gradient echo MRI (**b,** yellow arrow), the combined ^{18}F-FDG-PET-MRI shows the focal bone marrow lesion (**c,** yellow arrow) and the retroperitoneal lymph nodes next to the inferior vena cava (**c,** blue arrow). The simultaneously acquired DW-MRI demonstrates the focal bone marrow lesion on both $b=50$ s/mm^2 (**d,** yellow arrow) and $b=800$ s/mm^2 scans (**e,** yellow arrow). The retroperitoneal lymph nodes are depicted as well on both $b=50$ s/mm^2 (**d,** blue arrow) and $b=800$ s/mm^2 scans (**e,** blue arrow). The focal bone marrow metastasis in the vertebral body could be better detected on DW-MRI with a $b=800$ s/mm^2 compared to $b=50$ s/mm^2, in part due to an increased lesion-to-marrow contrast and in part due to suppression of the cerebrospinal fluid on the long b-value images. On the corresponding ADC map, however, the normal bone marrow and the focal bone marrow metastasis have a similar hypointense signal (**f,** yellow arrow). This could be due to the high iron content of the bone marrow

b-value and delta) in different studies, the ADC value of the normal bone marrow in our study was, expectedly, almost similar to the adults' values, in whom the mean ADC value of normal bone marrow was reported as $0.325 \pm 0.135 \times 10-3$ mm^2/s (range, 0.152–$0.542 \times 10-3$ mm^2/s) by Koutoulidis et al. [29]. Other investigators reported low ADC values at a younger age due to increased cellularity of the normal red marrow and higher ADC values during older age due to fatty conversion [30]. However, any causes of red marrow reconversion such as chemotherapy and administration of GCSF can also lead to decreased ADC values.

Accordingly, we found a wide range in ADC values of the normal bone marrow in our patients. There are multiple factors that influence the ADC value of the normal, non-neoplastic bone marrow. These include the proportion of hematopoietic marrow and fatty conversion, cell density of the normal bone marrow, patient age, iron content, and drug treatment (e.g., treatment with GCSF).

We found that bone marrow metastases had higher SNR compared to the normal bone marrow at both $b=50$ s/mm^2 and $b=800$ s/mm^2 on baseline and post-treatment scans which resulted in high diagnostic accuracy of DW-MRI in the detection of bone marrow metastases. This finding is in accordance with previously published studies [30, 31] and is likely attributed to the high cellularity and high proton density of tumors which results in prolongation of T1 and T2 relaxation times, and consequently, higher signal intensity of tumors compared to the normal bone marrow [30]. In a study of 46 adult patients, Geith et al. reported a higher performance of DW-MRI in the differentiation of benign and malignant vertebral body fractures with $b=100$, 250, and 400 s/mm^2 (low-to-intermediate b values) compared to $b=400$ and 600 s/mm^2 (intermediate-to-high b values) [32]. The underlying reason was probably a detection of T2-shine through effects from the random motion of free water molecules in the edema associated with a vertebral body fracture. However, in another organ system, the kidney, Erbay et al. reported a higher accuracy of the differentiation of benign and malignant renal lesions on DW-MR images with $b=800$ s/mm^2 compared to $b=50$ s/mm^2 in 60 adult patients [33]. This is based on the fact that most malignant tumors have a higher cell density (and hence, restricted diffusion)
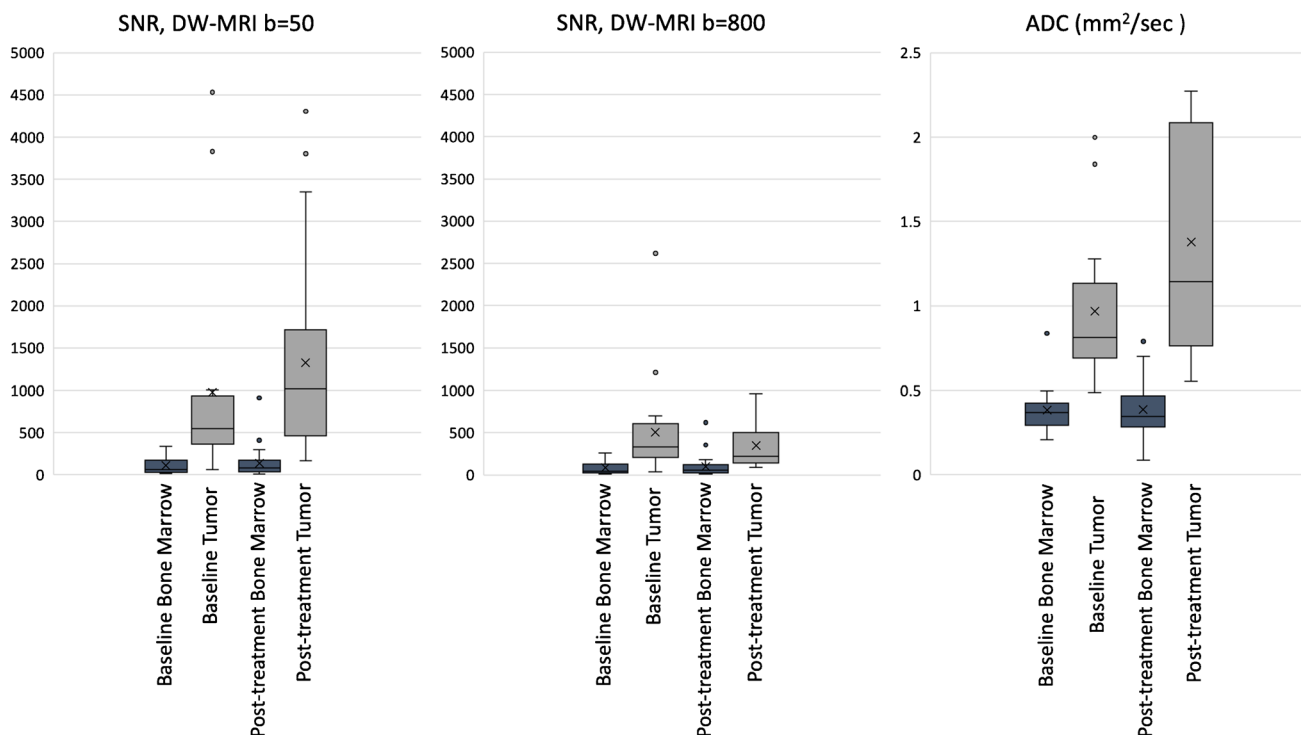
Fig. 5 Signal-to-noise ratios (SNR) of bone marrow and tumors on $b = 50$ s/mm^2 and $b = 800$ s/mm^2 DW-MRI scans and apparent diffusion coefficients (ADC) on the corresponding ADC maps using box plots **DW-MRI:** SNR of bone marrow metastases (tumor) are significantly higher compared to the SNR of normal bone marrow on the baseline and post-treatment scans ($p < .001$, respectively) at both $b = 50$ s/mm^2 and $b = 800$ s/mm^2 DW-MRI scans. On post-treatment scans, the SNR of normal bone marrow ($p = .045$) and of bone marrow metastases ($p < .001$) is significantly higher on $b = 50$ s/mm^2 compared to $b = 800$ s/mm^2 scans. **ADC map:** The corresponding ADC values of bone marrow metastases (tumor) are significantly higher compared to the ADC value of normal bone marrow on baseline and post-treatment scans ($p < .001$, respectively). The fences indicate the standard deviation and "x" indicate the median
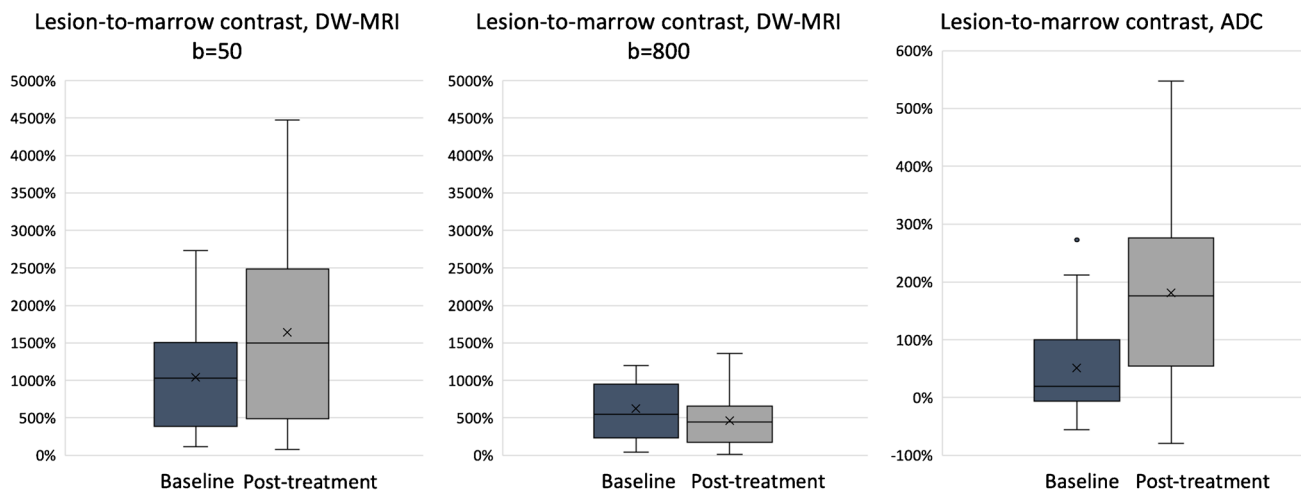

Fig. 6 Quantitative evaluation of the tumor-to-marrow contrast on $b = 50$ s/mm^2 and $b = 800$ s/mm^2 DW-MRI scans and ADC values on the corresponding ADC map using box plots. **DW-MRI:** The tumor-to-marrow contrast, measured as the difference between the tumor SNR and normal bone marrow SNR, was not statistically significant between baseline and post-treatment scans at $b = 50$ s/mm^2 ($p = .076$) and $b = 800$ s/mm^2 ($p = .653$). **ADC map:** The lesion-to-marrow contrast on the corresponding ADC map is significantly larger on post-treatment scans compared to the baseline scans ($p = .015$). The fences indicate the standard deviation and "x" indicate the median
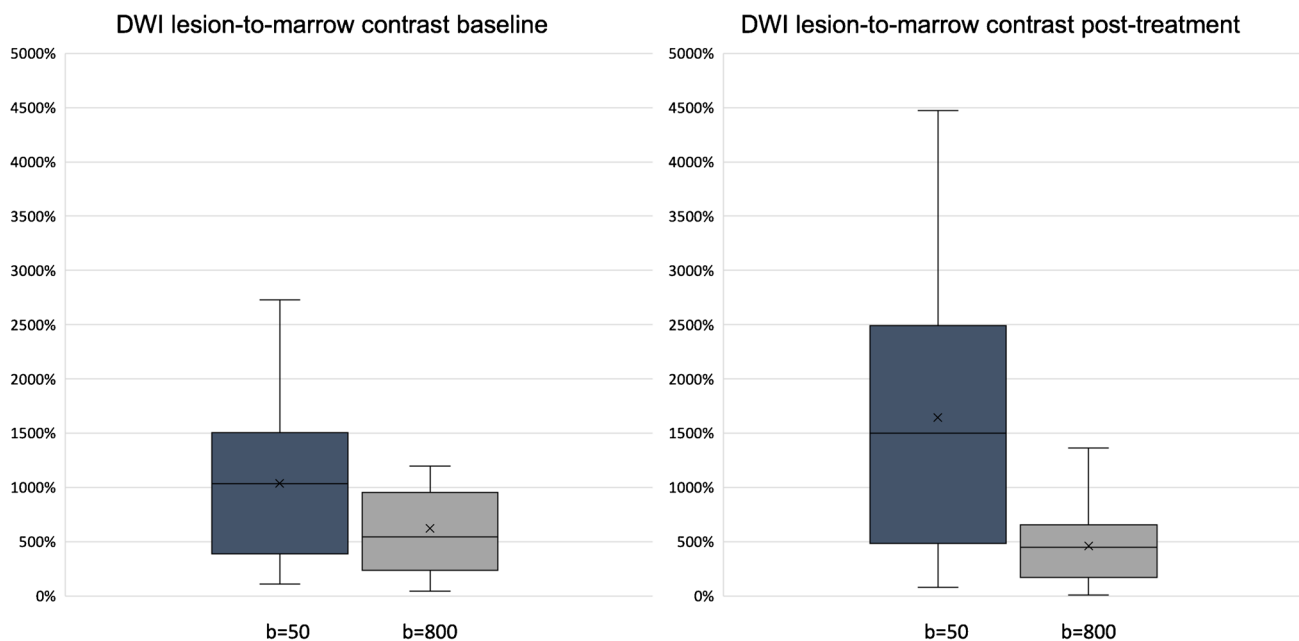
Fig. 7 Comparison of the tumor-to-marrow contrast on $b = 50$ s/mm^2 and $b = 800$ s/mm^2 at baseline and post-treatment DW-MRI scans map using box plots. The tumor-to-marrow contrast was larger on $b = 50$ s/mm^2 than $b = 800$ s/mm^2 DW-MRI scans on the baseline ($p = .009$) and post-treatment ($p < .001$) scans. The fences indicate the standard deviation and "x" indicate the median

compared to benign lesions. For distinguishing the benign and malignant bone lesions in adult patients, Liu et al. suggested using the b value in the range of 750 to 1000 s/mm^2 [34].

Also, we found an inverse signal intensity of reconverted bone marrow on ^{18}F-FDG-PET and DW-MRI scans. Recently, it has been noted that ^{18}F-FDG-PET can miss some bone marrow lesions, especially in reconverted hematopoietic marrow after chemotherapy [14]. This finding demonstrates the advantage of DW-MRI in the evaluation of post-treatment scans where reconverted bone marrow could mask the bone marrow lesions on ^{18}F-FDG-PET scans. This is important in the interpretation of children's PET images after treatment with chemotherapy [12] and GCSF [13], where the hypermetabolic normal hypercellular marrow can also mask the detection of focal lesions [11]. However, ^{18}F-FDG-PET can have advantages over DW-MRI scans in the detection of lesions in small bones, e.g., the ribs or clavicles, which are difficult to evaluate with MRI due to partial volume averaging.

The overall confidence of readers in the differentiation of bone marrow metastases and normal bone marrow was not significantly different between DW-MRIs with two b values in our study. This was in contrast to Liu et al.'s findings in adult patients who found higher diagnostic performance for DW-MRI with $b > 750$ s/mm^2 [34]. We also found a minor advantage of the $b = 800$ s/mm^2 images in the evaluation of three patients with spinal lesions. This finding was most likely due to the suppression of the T2 shine-through effect

of the spinal CSF on DW-MRI scans with a longer b-value [35], which improved the detection of small marrow lesions in the spine. This is of practical importance since most spinal metastatic lesions arise from the lamina or pedicles close to the CSF space. Thus, at lower b values such as 50 s/mm^2, the T2 shine-through effects of CSF predominate; in other words, the CSF appears to be bright, masking small metastatic lesions. However, at higher b values such as 800 s/mm^2, the T2 shine-through effects of the CSF are suppressed resulting in better delineation of metastatic lesions. Nonetheless, the quantitative evaluation of images showed a superior lesion-to-marrow contrast on $b = 50$ s/mm^2 images. Surprisingly, in the corresponding ADC map, the focal bone marrow metastases and normal bone marrow were both hypointense, and the focal bone marrow metastases could not be delineated. A mismatch of high tumor-to-marrow contrast on DWI images but close to no contrast on ADC maps could be due to high cellular marrow or high iron content of the normal bone marrow [26]. This highlights that the ADC map could be misleading in the evaluation of bone marrow metastases in children and young adults and should be used with caution while interpreting DW-MR images, specifically in younger patients with more cellular marrow. Nevertheless, changes in ADC values of a given lesion over time could still be useful for treatment monitoring purposes [36, 37].

We recognize several limitations of our study. The group of patients examined here was small and heterogenous, which limited statistical analyses. However, bone marrow metastases are seen in less than 10% of children with solid

extracranial cancers [38, 39] and are thus rare. Our study also lacks high enough patients from a particular tumor type, hence limiting our ability to determine if the conspicuity of the lesions on the DW-MRI is dependent on the tumor type. Nevertheless, to our knowledge, this is the largest cohort of pediatric patients with bone marrow metastases examined on DW-MRI. We used the combined DW-MRI with PET/MRI technologies for hybrid imaging. However, the high cost of PET/MRI scanners and the rarity of machines are major limitations for such combined applications. To circumvent this problem, sequential MRI and PET scan with secondary fusion can be considered when there is a lack of a combined PET/MRI system. Future studies must show if the FDG-PET part provides crucial additional information or if some patients could be examined with DW-MRI only.

In summary, DW-MRI with $b = 50$ s/mm^2 and $b = 800$ s/mm^2 can detect bone marrow metastases with high diagnostic accuracy and help detect early metastatic lesions in pediatric and young adult patients. DW-MRI scans with $b = 50$ s/mm^2 have superior lesion-to-marrow contrast. Also, ADC maps can be misleading for lesion detection or characterization in pediatric and young adult patients.

Data Availability Data generated or analyzed during the study are available from the corresponding author by request.

Declarations

Ethical approval All procedures performed in studies involving human participants were in accordance with the ethical standards of the institutional and/or national research committee and with the 1964 Helsinki declaration and its later amendments or comparable ethical standards.

Conflict of interest The authors declare no competing interests.

References

1. Jambor I, Kuisma A, Ramadan S, Huovinen R, Sandell M, Kajander S, et al. Prospective evaluation of planar bone scintigraphy, SPECT, SPECT/CT, 18F-NaF PET/CT and whole body 1.5T MRI, including DWI, for the detection of bone metastases in high risk breast and prostate cancer patients: SKELETA clinical trial. Acta Oncol. 2016;55(1):59–67.

2. Mayerhoefer ME, Karanikas G, Kletter K, Prosch H, Kiesewetter B, Skrabs C, et al. Evaluation of diffusion-weighted magnetic resonance imaging for follow-up and treatment response assessment of lymphoma: results of an 18F-FDG-PET/CT-Controlled Prospective Study in 64 Patients. Clin Cancer Res. 2015;21(11):2506–13.

3. Lee JH, Yoo GS, Yoon YC, Park HC, Kim HS. Diffusion-weighted and dynamic contrast-enhanced magnetic resonance imaging after radiation therapy for bone metastases in patients with hepatocellular carcinoma. Sci Rep. 2021;11(1):10459.

4. de Oliveira AD, de Souza GHY, Guimarães C, Guimarães MD, da Costa CML, Porto FHG, et al. Evaluation of whole-body MRI with diffusion-weighted sequences in the staging of pediatric cancer patients. PLoS ONE. 2020;15(8):e0238166.

5. Ishiguchi H, Ito S, Kato K, Sakurai Y, Kawai H, Fujita N, et al. Diagnostic performance of (18)F-FDG PET/CT and whole-body diffusion-weighted imaging with background body suppression (DWIBS) in detection of lymph node and bone metastases from pediatric neuroblastoma. Ann Nucl Med. 2018;32(5):348–62.

6. Theruvath AJ, Siedek F, Muehe AM, Garcia-Diaz J, Kirchner J, Martin O, et al. Therapy response assessment of pediatric tumors with whole-body diffusion-weighted MRI and FDG PET/MRI. Radiol. 2020;296(1):143–51.

7. Baliyan V, Das CJ, Sharma R, Gupta AK. Diffusion weighted imaging: technique and applications. World J Radiol. 2016;8(9):785–98.

8. Siegel MJ, Jokerst CE, Rajderkar D, Hildebolt CF, Goyal S, Dehdashti F, et al. Diffusion-weighted MRI for staging and evaluation of response in diffuse large B-cell lymphoma: a pilot study. NMR Biomed. 2014;27(6):681–91.

9. Padhani AR, Liu G, Koh DM, Chenevert TL, Thoeny HC, Takahara T, et al. Diffusion-weighted magnetic resonance imaging as a cancer biomarker: consensus and recommendations. Neoplasia. 2009;11(2):102–25.

10. White NS, McDonald C, Farid N, Kuperman J, Karow D, Schenker-Ahmed NM, et al. Diffusion-weighted imaging in cancer: physical foundations and applications of restriction spectrum imaging. Cancer Res. 2014;74(17):4638–52.

11. Nonomura Y, Yasumoto M, Yoshimura R, Haraguchi K, Ito S, Akashi T, et al. Relationship between bone marrow cellularity and apparent diffusion coefficient. J Magn Reson Imaging. 2001;13(5):757–60.

12. Daldrup-Link HE, Henning T, Link TM. MR imaging of therapy-induced changes of bone marrow. Eur Radiol. 2007;17(3):743–61.

13. Fletcher BD, Wall JE, Hanna SL. Effect of hematopoietic growth factors on MR images of bone marrow in children undergoing chemotherapy. Radiol. 1993;189(3):745–51.

14. Rashidi A, Baratto L, Theruvath AJ, Greene EB, Hawk KE, Lu R, et al. Diagnostic Accuracy of 2-[(18)F]FDG-PET and whole-body DW-MRI for the detection of bone marrow metastases in children and young adults. Eur Radiol. 2022;32:4967.

15. Gasparil ADI, Gupta H, Sheybani E, Chavhan GB. Low b-value (50–100) diffusion-weighted images detect significantly more hyperintense liver lesions in children than T2-weighted images. Pediatr Radiol. 2019;49(10):1299–305.

16. Benjamini Y, Hochberg Y. Controlling the false discovery rate: a practical and powerful approach to multiple testing. J Roy Stat Soc: Ser B (Methodol). 1995;57(1):289–300.

17. Green P, MacLeod CJ. SIMR: an R package for power analysis of generalized linear mixed models by simulation. Methods Ecol Evol. 2016;7(4):493–8.

18. Cohen J. Weighted kappa: nominal scale agreement with provision for scaled disagreement or partial credit. Psychol Bull. 1968;70(4):213–20.

19. Landis JR, Koch GG. The measurement of observer agreement for categorical data. Biometrics. 1977;33(1):159–74.

20. Oberlin O, Rey A, Lyden E, Bisogno G, Stevens MC, Meyer WH, et al. Prognostic factors in metastatic rhabdomyosarcomas: results

of a pooled analysis from United States and European cooperative groups. J Clin Oncol. 2008;26(14):2384–9.

21. Paulussen M, Ahrens S, Burdach S, Craft A, Dockhorn-Dworniczak B, Dunst J, et al. Primary metastatic (stage IV) Ewing tumor: survival analysis of 171 patients from the EICESS studies. European Intergroup Cooperative Ewing Sarcoma Studies. Ann Oncol. 1998;9(3):275–81.

22. Cesari M, Righi A, Colangeli M, Gambarotti M, Spinnato P, Ferraro A, et al. Bone marrow biopsy in the initial staging of Ewing sarcoma: experience from a single institution. Pediatr Blood Cancer. 2019;66(6):e27653.

23. Purz S, Mauz-Körholz C, Körholz D, Hasenclever D, Krausse A, Sorge I, et al. [18F]Fluorodeoxyglucose positron emission tomography for detection of bone marrow involvement in children and adolescents with Hodgkin's lymphoma. J Clin Oncol. 2011;29(26):3523–8.

24. Yağci-Küpeli B, Koçyiğit-Deveci E, Adamhasan F, Küpeli S. The value of 18F-FDG PET/CT in detecting bone marrow involvement in childhood cancers. J Pediatr Hematol Oncol. 2019;41(6):438–41.

25. Badr S, Kotb M, Elahmadawy MA, Moustafa H. Predictive value of FDG PET/CT versus bone marrow biopsy in pediatric lymphoma. Clin Nucl Med. 2018;43(12):e428–38.

26. Ording Müller LS, Avenarius D, Olsen OE. High signal in bone marrow at diffusion-weighted imaging with body background suppression (DWIBS) in healthy children. Pediatr Radiol. 2011;41(2):221–6.

27. Ibrahim YA, Elsadawy ME, El Naggar T. Role of quantitative diffusion-weighted imaging in differentiation between red and infiltrated marrow in pediatric patients with hematologic malignancy. Egypt J Radiol Nuclear Med. 2019;50(1):13.

28. Tschischka A, Schleich C, Boos J, Eichner M, Schaper J, Aissa J, et al. Age-related apparent diffusion coefficients of lumbar vertebrae in healthy children at 1.5 T. Pediatr Radiol. 2018;48(7):1008–12.

29. Koutoulidis V, Fontara S, Terpos E, Zagouri F, Matsaridis D, Christoulas D, et al. Quantitative diffusion-weighted imaging of the bone marrow: an adjunct tool for the diagnosis of a diffuse MR imaging pattern in patients with multiple myeloma. Radiol. 2017;282(2):484–93.

30. Padhani AR, van Ree K, Collins DJ, D'Sa S, Makris A. Assessing the relation between bone marrow signal intensity and apparent diffusion coefficient in diffusion-weighted MRI. AJR Am J Roentgenol. 2013;200(1):163–70.

31. Eiber M, Holzapfel K, Ganter C, Epple K, Metz S, Geinitz H, et al. Whole-body MRI including diffusion-weighted imaging (DWI) for patients with recurring prostate cancer: technical feasibility and assessment of lesion conspicuity in DWI. J Magn Reson Imaging. 2011;33(5):1160–70.

32. Geith T, Schmidt G, Biffar A, Dietrich O, Duerr HR, Reiser M, et al. Quantitative evaluation of benign and malignant vertebral fractures with diffusion-weighted MRI: what is the optimum combination of b values for ADC-based lesion differentiation with the single-shot turbo spin-echo sequence? AJR Am J Roentgenol. 2014;203(3):582–8.

33. Erbay G, Koc Z, Karadeli E, Kuzgunbay B, Goren MR, Bal N. Evaluation of malignant and benign renal lesions using diffusion-weighted MRI with multiple b values. Acta Radiol. 2012;53(3):359–65.

34. Liu LP, Cui LB, Zhang XX, Cao J, Chang N, Tang X, et al. Diagnostic performance of diffusion-weighted magnetic resonance imaging in bone malignancy: evidence from a meta-analysis. Med (Baltimore). 2015;94(45):e1998.

35. Takahara T, Kwee TC. Low b-value diffusion-weighted imaging: emerging applications in the body. J Magn Reson Imaging. 2012;35(6):1266–73.

36. McDonald K, Sebire NJ, Anderson J, Olsen OE. Patterns of shift in ADC distributions in abdominal tumours during chemotherapy-feasibility study. Pediatr Radiol. 2011;41(1):99–106.

37. Demir S, Altinkaya N, Kocer NE, Erbay A, Oguzkurt P. Variations in apparent diffusion coefficient values following chemotherapy in pediatric neuroblastoma. Diagn Interv Radiol. 2015;21(2):184–8.

38. Levis A, Pietrasanta D, Godio L, Vitolo U, Ciravegna G, Di Vito F, et al. A large-scale study of bone marrow involvement in patients with Hodgkin's lymphoma. Clin Lymphoma. 2004;5(1):50–5.

39. Cotterill SJ, Ahrens S, Paulussen M, Jürgens HF, Voûte PA, Gadner H, et al. Prognostic factors in Ewing's tumor of bone: analysis of 975 patients from the European Intergroup Cooperative Ewing's Sarcoma Study Group. J Clin Oncol. 2000;18(17):3108–14.